Japan Architectural Review
Open Access
Architectural Institute of Japan

Translated Paper

Analytical study of the main causes of damage to pile foundations during the 2011 off the Pacific coast of Tohoku earthquake

Osamu Kaneko,[1] Shiori Kawamata,[2] Shoichi Nakai,[3] Toru Sekiguchi[4] and Tomohisa Mukai[5]

[1]Technical Research Center, Toda Corporation, Tokyo, Japan; [2]Japan Pile Corporation, Tokyo, Japan; [3]Chiba University, Chiba, Japan; [4]Graduate School of Engineering, Chiba University, Chiba, Japan; [5]Building Research Institute, Tsukuba-shi, Ibaraki, Japan

Correspondence
Osamu Kaneko, Technical Research Center, Toda Corporation, Tokyo, Japan.
Email: osamu.kaneko2@toda.co.jp

Funding information
No funding information is provided.

The Japanese version of this paper was published in Volume 80 Number 717, pages 1699-1706, https://doi.org/10.3130/aijs.80.1699 of *Journal of Structural and Construction Engineering (Transactions of AIJ)*. The authors have obtained permission for secondary publication of the English version in another journal from the Editor of *Journal of Structural and Construction Engineering (Transactions of AIJ)*. This paper is based on a translation of the Japanese version with slight modifications.

Received October 12, 2017; Accepted February 5, 2018

doi: 10.1002/2475-8876.12033

Abstract

The authors performed static analyses using a foundation structure model to simulate the process leading to distinctive damage to pile foundations during the 2011 off the Pacific coast of Tohoku earthquake. Notable aspects of the analytical method used for this simulation include consideration of the nonlinear load-deformation characteristics of pile elements, the dependence of the rotational stiffness at the pile head on the axial load, and the nonlinear behavior of soil spring including the pile group effect. The results of the simulations of pile failure for each loading direction provide a useful explanation of the observed damage to pile foundations. The proposed analysis method can be considered a practical approach to the seismic design of foundations subject to severe earthquakes.

Keywords
earthquake damage, pile foundation, pile group effect, pile head connection, the 2011 off the Pacific coast of Tohoku earthquake

1. Introduction

Strong ground shaking during the 2011 off the Pacific coast of Tohoku earthquake (the 2011 Great East Japan Earthquake) damaged pile foundations over wide areas in Miyagi and Chiba prefectures in addition to causing various other forms of foundation damage through liquefaction-induced ground deformation, slope failure and complete destruction by tsunami. Such damage to pile foundations, which has been commonly observed in past major earthquakes, resulted in building structure tilting even though superstructures remained practically intact. Pile foundation repair and careful jacking-up to level were required to restore the buildings for use.

Most of the damaged buildings were constructed before the Japanese code requirements for the seismic design of foundations went into effect in 1985, while several of them were constructed after 1985. According to the damage investigation,[1] 74% of the damaged buildings were constructed before 1985. Since approximately 26% of the damage occurred in buildings constructed since 1985, the year of construction does not appear to be a crucial factor in the damage to piles. In addition, pile damage notably occurred in precast concrete piles known to have non-ductile deformation characteristics, and the soil in which damage was observed consisted of very soft clay, a liquefiable layer and/or non-homogeneous strata in most cases. These conditions indicate that significant effects of nonlinear behavior of piles and soil materials must be considered when simulating the pile failure process.

The authors focused on a case in which pile damage resulted in building tilting although the pile foundation design was based on a simple linear elastic analysis in accordance with the existing design code in 1987. An analytical study was performed using a foundation structure model to simulate the distinctive pile failure modes observed during the 2011 off the Pacific coast of Tohoku earthquake.

In the analysis model, a remarkably damaged frame was removed and used as a calculation model consisting of piles with soil springs. Based on a previous study[2] on the seismic performance of pile foundations during severe earthquakes, nonlinear flexural rigidity of the pile element and rotational stiffness at the pile head were adopted. The nonlinear characteristics of the soil springs were also adjusted in accordance with soil type and depth (overburden pressure). In addition, the pile group effect was considered depending on the position and spacing of each pile in a group. The seismic response of

the building and the ground deformation were evaluated based on a free field ground response analysis using ground motions recorded at an observation point near the site. The inertia force and axial force at the pile heads were estimated based on the results of elastic analysis.

2. Outline of the analyzed building

2.1 Superstructures

Figure 1 shows the building foundation plan and the differential settlement of the footings, with the damaged piles designated by numbers. The target building[3] is an eight-storey residential building that is 23.4 m in height. The building consists of steel-reinforced concrete columns up to the fourth floor and reinforced concrete (RC) columns above. Shear walls are placed in the NS (north-south) direction except that baseline 4 is braced. In the EW (east-west) direction, simple filled-walls are attached to the building frame. Although the building has a nearly square plan with dimensions of 10.95 m × 12.9 m across grid points 1C to 3E, a heavy staircase and an elevator within grid points 3D to 4F make the building shape irregular. The building is a part of housing complex composed of 3 buildings connected with one another by expansion joints. After the earthquake, only the analyzed building was tilted.

2.2 Foundations

Forty pre-stressed, high-strength concrete (PHC) spun piles support the building (Figure 1). Two to five piles are placed in each pile cap at a spacing 2.5 times the pile diameter (500 mm). The design-allowable bearing capacity of each pile is assumed to be 960 kN. Pile length ranges from 30 to 33 m with the upper 7 m section consisting of a C-type element (concrete strength = 85 N/mm^2, pre-stress = 10 N/mm^2) and the remaining lower section consisting of an A-type element (concrete strength = 80 N/mm^2, effective pre-stress = 4 N/mm^2). Piles No. 5 and No. 17 have a joint connection that is 3-4 m higher than the designed level, which suggests the pile may have been cut off after installation. However, no damage was observed at the pile heads in these piles.

The pile heads are embedded 100 mm into the pile caps with 8 D13 rebars (Figure 2). It was confirmed that the piles were designed with an allowable stress design method that fulfilled the existing code.

2.3 Ground conditions

Figure 3 shows a typical soil profile at the site with soil types and *N*-value obtained by standard penetration tests (SPT *N*-value). The site consists of primarily clayey layers sandwiched between fine sand and gravel layers that extend approximately 28 m below the ground surface (GL-28m), with SPT *N*-values ranging from 3 to 30. Groundwater is noted at GL-0.95m. Piles are embedded into the sandy bearing layer with an SPT *N*-value greater than 60 identified at approximately GL-30m. Soil profiles of the vicinity show significant variation in stratigraphy, which indicates considerable uncertainty regarding subsurface soil conditions at the site.

2.4 Damage during the earthquake

The measured tilting of the building was 1 in 178 in the northwest direction, and the maximum relative settlement after the earthquake was 89 mm. Shear cracks observed in the superstructure were 0.2-0.5 mm wide on slabs and inner walls in addition to approximately 1.0 mm wide cracks in the exterior walls on the north and south sides (Figure 4). More severe damage appeared to be the spall-off of the cover concrete of the mullion walls between windows in the first, second and sixth stories. Damage was also observed at the expansion joint, which indicates collision between adjacent buildings at the south-east corner.

As damage to the superstructure was limited from a structural perspective, it was determined to repair the pile foundations and restore the building by means of the underpinning technique. Integrity tests (ITs) with direct visual and video-camera observations were conducted on the piles after ground excavation around the pile heads.

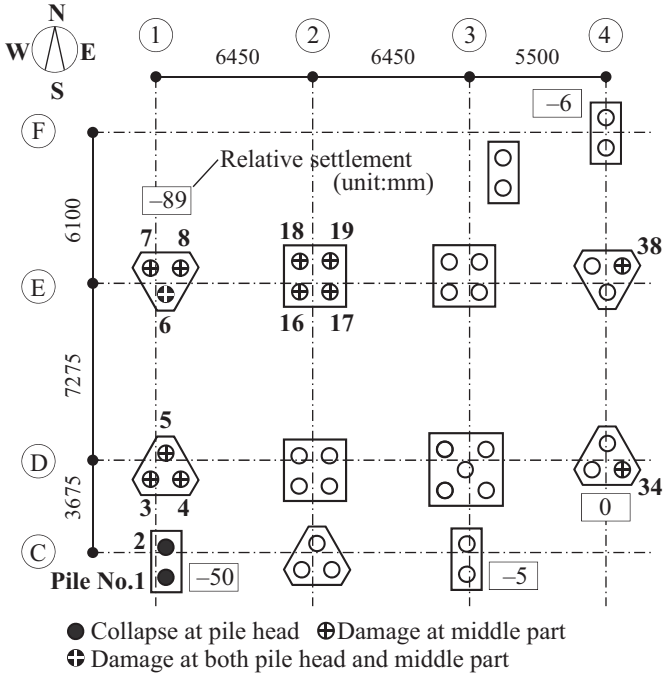

Figure 1. Pile layout and pile damage locations

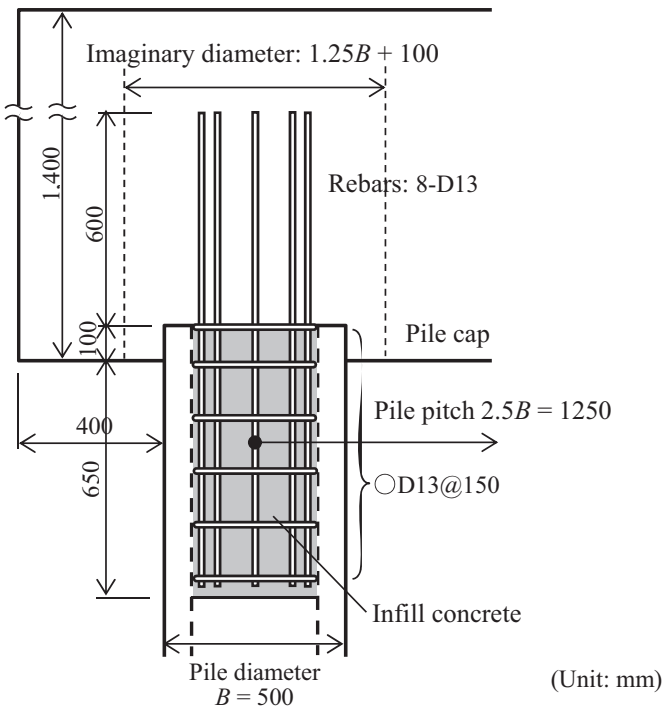

Figure 2. Detail of pile head

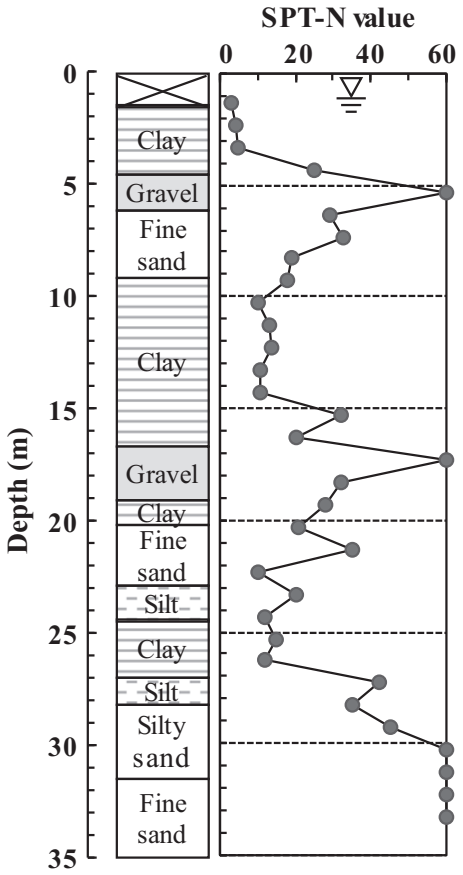

Figure 3. Soil profile

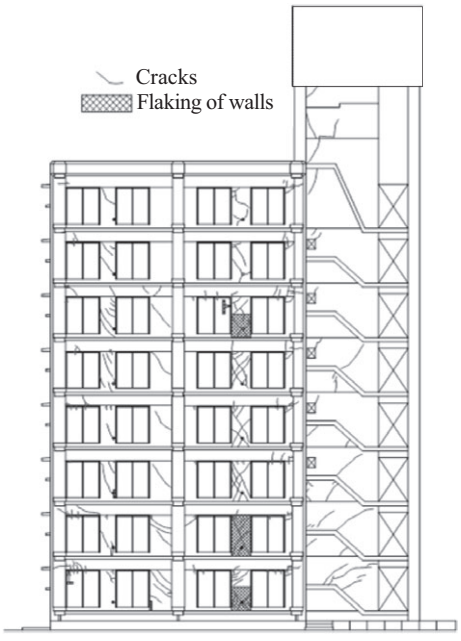

Figure 4. Damage to exterior walls on south side

Figure 5 shows the damage around the pile heads of Piles No. 1, 2, and 6. Investigation revealed that Piles No. 1, 2, and 6, denoted with filled circles in Figure 1, were heavily damaged at pile heads. Another 12 piles, denoted with crossed circles in Figure 1, were assessed to be broken around the middle of the pile. Fourteen piles in total were identified as damaged, with the remaining piles undamaged.

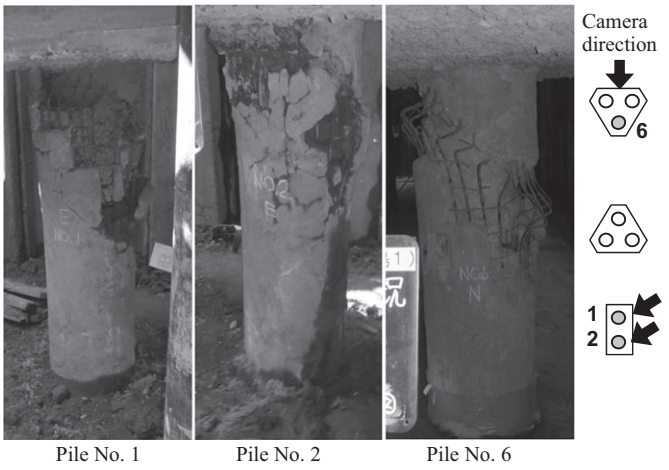

Figure 5. Damage to pile heads

Piles No. 1 and 2 exhibited compression failure or shear failure in the north-west direction, whereas a shear failure plane in the north-west direction was observed slightly below the pile head in Pile No. 6. Based on the ITs, the extent of the damaged sections below the pile heads is summarized in Table 1. Most of the damage occurred in the upper pile section. Video-camera observation indicated a complete break in tension of Pile No. 5 at 4.3 m depth and partial cracking of other piles.

3. Seismic analyses

3.1 Calculation model and set up of input loads

Figure 6 shows the analysis model of severely damaged piles along baseline 1. The model consists of 8 piles represented by

Table 1. Depth of damaged section from pile head

Pile no.	3	4	5	6	7	8	16-19	34	38
Depth (m)	5.1	5.3	4.4	3.3	6.0	6.1	7.3	4.2	4.7

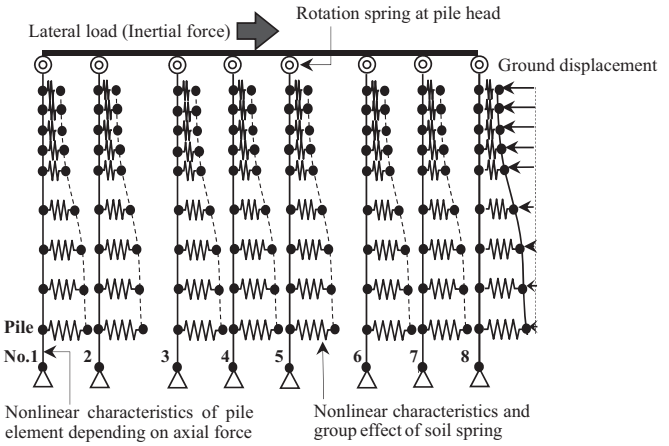

Figure 6. Analysis model

beam elements and a rotation spring at the top, along with nonlinear soil springs. Static push-over analyses are conducted on this model to simulate the damage process of piles. Pile elements are 30 m long with pin support at the pile tips. Beam element lengths in the upper parts are half of one pile diameter long, while those in lower parts are 0.5 or 1.0 m long.

The procedure used to calculate the lateral inertial force at the pile head from the superstructure and the kinematic force caused by ground displacement along the pile are schematically explained in Figure 7. First, a one-dimensional equivalent linear site response analysis is performed at the recording station to estimate the input motion at the engineering bedrock. The recorded ground motion at the ground surface (2 km from the building site) had a peak ground acceleration (PGA) of 7.46 m/s^2 in the east-west direction and 10.69 m/s^2 in the north-south direction. The recorded ground motion was obtained from the strong-motion seismograph network known as K-NET operated by the National Research Institute for Earth Science and Disaster Resilience in Japan. Then, the site-specific ground motion at the building site is calculated by a ground response analysis using the engineering bedrock motion as the input. Note that the engineering bedrock is assumed to be at the same depth at the building site and the recording station. Shear wave velocity (V_s) for the seismic response analysis is identified by micro-tremor measurements, available PS logging in neighboring sites, and the SPT N-value shown in Figure 3. The nonlinear soil behavior of each layer is based on a previous study[4] and dependent on soil type.

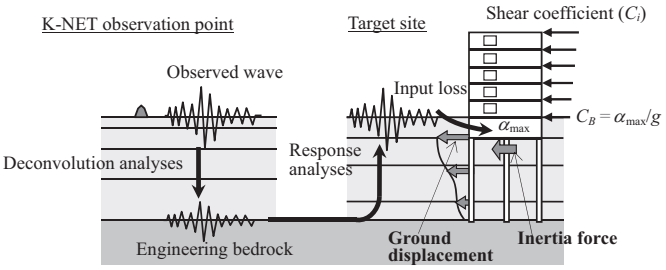

Figure 7. Estimation procedure of input static load

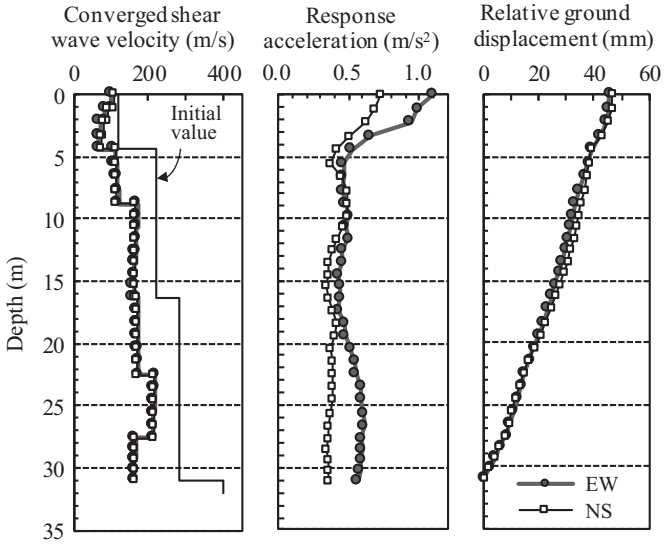

Figure 8. Results of response analyses

Maximum inertial force at the pile head is estimated by taking base shear coefficient C_B of the ground floor, which is calculated by dividing the maximum acceleration by the gravity acceleration (g) and allowing for kinematic interaction.[5] The maximum response acceleration divided by g is 0.41 in the north-south direction and 0.54 in the east-west direction. Considering frequency dependency, the kinematic interaction is equivalent to 51% and 55% of the maximum acceleration. However, C_B in the east-west direction is reduced to 0.34 in the analyses, considering the actual damage to the superstructure. Maximum values of the lateral force and axial force at the pile head are obtained from the static elastic analysis of the superstructure using multi-frame (a structural analysis program), in which the shear force at each floor is assumed to be distributed according to the Japanese structural design code. Ground displacement is assumed to be relative to the pile tip, and based on the maximum displacement profile from the ground response analysis. Input lateral load due to inertia and the effect of ground displacement are applied simultaneously in the same direction. The displacement is divided into 30 equal steps in the static push-over analysis.

Figure 8 shows the distribution of the initial values of V_s with their converged V_s value after degradation of the soil stiffness, together with PGA and relative ground displacement.

3.2 Modeling of soil spring

The relationship between the lateral subgrade reaction (P) and the soil deformation around the piles (δ) is modeled as a polygonal line through Equations (1) and (2), as proposed by Mase and Nakai.[6] Respective values are determined the using parameters shown in Table 2. Pile group effects on nonlinear soil springs are considered with respect to the relative position of piles in the loading direction (either front side or back side) and spacing as follows:

$$\frac{R(R)}{\delta(R)} = \frac{K_0}{1 + \frac{K_0}{P_{max}} \frac{(1-R_e)}{u} \frac{2}{\pi} \ln\left\{\sec\left(\frac{\langle R-R_e\rangle}{1-R_e}\frac{\pi}{2}\right)\right\}} \quad (1)$$

Table 2. Soil spring parameters

No.	Depth of lower end (m)	Soil classification	Initial V_{s0} (m/s)	Converged V_{s1} (m/s)	Average SPT N-value	ϕ	C_u (kN/m^2)	u
1	3.3	Clay	120	77.8	4.5	0	30	20
2	4.4	Clay	120	66.8	25.0	0	156	20
3	8.8	Sand	220	116.4	27.0	40	0	50
4	16.3	Clay	220	167.2	16.1	0	113	50
5	22.5	Sand	280	173.4	27.6	36.7	0	50
6	27.6	Clay	280	216.2	14.8	0	105	100
7	33.0	Sand	280	165.7	43.0	0	281	100

$$K_0 = \xi 1.3 \frac{E_s}{(1-\nu^2)} \left(\frac{E_s B^4}{EI}\right)^{1/12} \quad (2)$$

where R is P normalized by the maximum value of the lateral subgrade reaction (P_{max} or P_y), R_e is R at the elastic limit (here, 0), ν is Poisson's ratio of soils, B is the pile diameter, and EI is the flexural rigidity of the pile.

The soil stiffness (E_s) used to calculate the initial spring constant (K_0) is estimated as a converged value of shear stiffness obtained by the seismic response analyses. Pile group coefficient ξ is applied to the soil stiffness of all piles according to the ratio of pile spacing R_p/B by Equations (3) and (4).

$$\xi = 0.15\frac{R_p}{B} + 1.0 \quad \text{when} \frac{R_p}{B} \le 6.0 \quad (3)$$

$$\xi = 1.0 \quad \text{when} \frac{R_p}{B} > 6.0 \quad (4)$$

P_y is calculated by Equations (5)-(8)[7] according to soil type and depth z. The internal friction angle (ϕ) and cohesion (C_u) in these equations are estimated using empirical correlation[8].

For sandy soil above a certain depth (termed area 1) where the wedge of soil in front of the lead piles tends to move toward the surface under the lateral load acting on piles,

$$P_y = \kappa\gamma z\left\{\frac{K_0 \tan\phi \sin\phi}{\tan(\beta-\phi)}\frac{z}{B} + \frac{\tan\beta}{\tan(\beta-\phi)}\left(1+\frac{z}{B}\tan\beta\tan\alpha\right) + K_0\tan\beta(\tan\phi\sin\beta - \tan\alpha)\frac{z}{B} - K_A\right\} \quad (5)$$

For sandy soil below a certain depth (termed area 2) where soil tends to move horizontally,

$$P_y = \kappa F_\phi \gamma z, \quad F_\phi = \frac{\cos\left(\frac{\pi}{4}-\frac{\phi}{2}\right)}{\cos\left(\frac{\pi}{4}+\frac{\phi}{2}\right)}\frac{1-\sin\phi}{\cos\phi}e^{\left(\frac{2\pi}{3}-\phi\right)\tan\phi} - K_A \quad (6)$$

For clayey soil in area 1,

$$P_y = \gamma z + 2C_u + 2\lambda\frac{z}{B}C_u \quad (7)$$

For clayey soil in area 2,

$$P_y = \lambda C_u \quad (8)$$

P_y for the piles in the back is also reduced considering pile group effects using Equations (9)-(11)[9].

$$\kappa = (0.55 - 0.007\phi)\left(\frac{R_p}{B} - 1.0\right) + 0.4 \quad \text{for sand, upper limit of } \kappa \text{ is } 3.0 \quad (9)$$

$$\mu = 0.6\frac{R_p}{B} - 0.4, \lambda = 3.0\frac{R_p}{B} \text{ for clay when} \frac{R_p}{B} < 3.0 \quad (10)$$

$$\mu = 1.4, \lambda = 9.0 \text{ for clay when} \frac{R_p}{B} \ge 3.0 \quad (11)$$

where K and K_A are the at-rest and active earth pressure coefficients, respectively, α and β are the wedge angles at failure, here $\alpha = \phi/2$ and $\beta = \pi/4 + \phi/2$, and γ is the unit weight of the soil.

Coefficient u, which represents the extent of approaching the ultimate ground reaction force, and the larger the value, the closer the plastic state approaches earlier. The values in Table 2 are estimated depending on the depth with reference to a simulation of loading tests of piles. Figure 9 shows typical examples of the nonlinear soil spring model for Pile No. 1 at the clay and sand layers.

3.3 Modeling of pile-to-pile head connection

The load-displacement characteristics of the pile-to-pile head connection are estimated employing fiber elements analysis[10] while maintaining a constant axial load. The bending moment M and curvature φ relationship for the pile is represented by a tri-linear model,[11] with crack moment M_c and yield moment M_y as break points in the tri-linear curve. Based on structural experiments[12] on RC columns under 600-2500 kN axial force, the pile head connection is modeled by a bi-linear curve with yield moment M_y as a break point. In this case, M_y is calculated considering an imaginary diameter concept[13] by adding 100 mm to 1.25 times of the pile diameter (Figure 2). The rotation angle is obtained by multiplying the calculated curvature by the pile diameter. Nominal values are considered while calculating these material properties. Figures 10 and 11 show estimated characteristics for the portion of the pile close to the pile head and the pile head connection, respectively.

Shear capacity Q_u of the PHC pile is estimated by Equation (12), which is commonly employed in structural design. It is confirmed that the empirical formula proposed by Kishida et al[14] provides values similar to those based on Equation (12) under the targeted range of the shear span ratio or axial force σ_g:

$$Q_u = \frac{2tl}{S_0}\frac{1}{2}\sqrt{(\sigma_g + 2\phi\sigma_t)^2 - \sigma_g^2} \quad (12)$$

where σ_g is obtained by adding the effective pre-stress of the pile to the axial load, t is the thickness of a hollow pile, S_0 and I are the first and secondary moment of area, respectively, σ_t is tensile strength and ϕ is the ratio of σ_t and slant tensile stress at shear failure, 0.5.

4. Results of analyses

4.1 Analysis cases

The analyzed cases are summarized in Table 3. The authors focused on 2 phases up to failure considering the pile position and the direction of failure identified in the damage investigation.

Phase 1: The pile heads of Piles No. 1 and 2 reach compressive or shear failure caused by north-to-south loading with excessive axial force. This phase is termed Case1.

Phase 2: The pile head of Pile No. 6 and middle part of Piles No. 3 to 8 reach failure caused by west-to-east loading (Case 2) or reverse loading (Case 3).

Phase 1 is divided into 2 stages. The first stage, termed Case 1-1, is the period until the pile head of Pile No. 1 is broken, after which the lateral load is redistributed to the remaining piles. Following the first stage, 3 separate cases are considered in the second stage, including the case in which Pile No. 1 maintains the pile group effect (Case 1-2A), and the case in which the pile group effect is lost, which make Pile No. 2 a front pile (Case 1-2B). In the latter scenario, the case in which

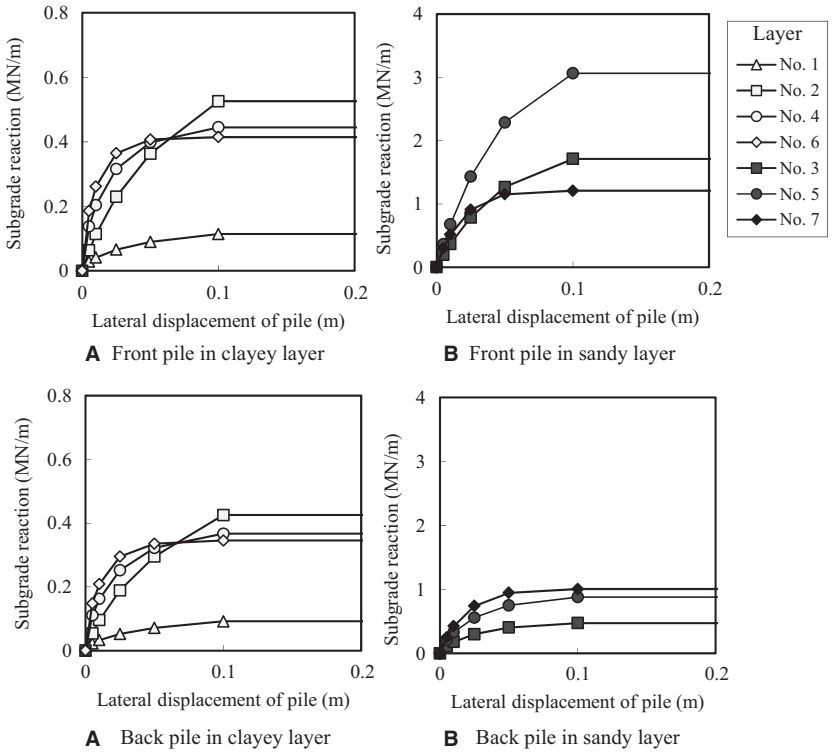

Figure 9. Soil spring model (Pile No. 1/north-to-south direction)

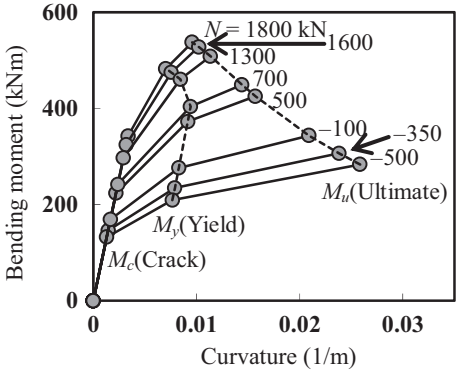

Figure 10. Relationship of bending moment and curvature of pile element

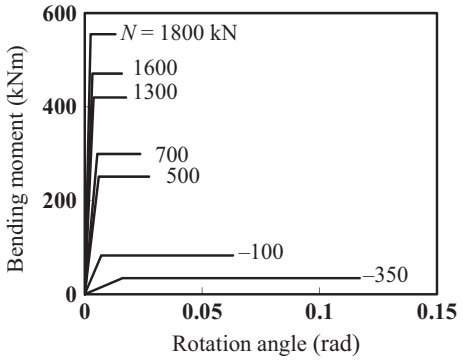

Figure 11. Relationship of bending moment and rotation angle at pile head connection

the axial force of Pile No. 1 is transferred to Pile No. 2 is termed Case 1-2C. In addition to these analyses, linear elastic analysis for a single pile is performed based on the current design code (Case 0). In this case, both the pile and the soil remain elastic, and the coefficient of the subgrade reaction (k_h) is estimated by Equations (13) and (14),[15] which are widely used in elastic design.

$$k_{h0} = \alpha E_0 B^{-\frac{3}{4}} \tag{13}$$

$$k_h = k_{h0} y^{-\frac{1}{2}} \tag{14}$$

where k_{h0} is the value at 10 mm lateral displacement of the pile (y) (in this equation, a non-dimensional value), α is an empirical constant depending on soil type (which is 80 for sand or 60 for clay). Soil stiffness E_0 is calculated using the SPT N-value (N) and the relation in $E_0 = 700\ N$.

4.2 Results of North-to-South loading in Cases 1-1 and 1-2

Figure 12 shows the bending moment and shear force distribution along the pile of Piles No. 1, 2, and 6 obtained in Case 1-1 at $C_B = 0.36$, where Pile No. 1 reaches initial shear failure. At this step, the bending moment at the pile head of Piles No. 2 and 6 reaches approximately 80% of the yielding value, while the bending moment in all the piles except Piles No. 1, 2 and 6 remains just after reaching the crack moment throughout the depth. Note that the double lines between 4 to 7 m in depth reflect the possible range of pile capacity in consideration of the joint depth.

Figure 13 shows the similar results of Piles No. 2 and 6 in Cases 1-2A, 1-2B and 1-2C at $C_B = 0.39$, in which the vertical load supported by Pile No. 1 is redistributed to other piles. In Case 1-2B, where the pile group effect on Pile No. 2 is neglected, both Piles No. 2 and No. 6 reach shear capacity. In

Table 3. Analysis condition

		Axial force (kN)							
Case	Load direction	Pile no. 1	Pile no. 2	Pile no. 3	Pile no. 4	Pile no. 5	Pile no. 6	Pile no. 7	Pile no. 8
1-1	N to S	1300	1300	700	700	700	500	500	500
1-2A	N to S	-	1300	700	700	700	500	500	500
1-2B	N to S	-	1300	700	700	700	500	500	500
1-2C	N to S	-	2600	700	700	700	500	500	500
2	W to E	-	-	−350	−350	−350	−100	−100	−100
3	E to W	1800	1800	1600	1600	1600	1600	1600	1600
0	-	Excluding							

Filled squares mean that they are the piles in the back considering the pile group effect.

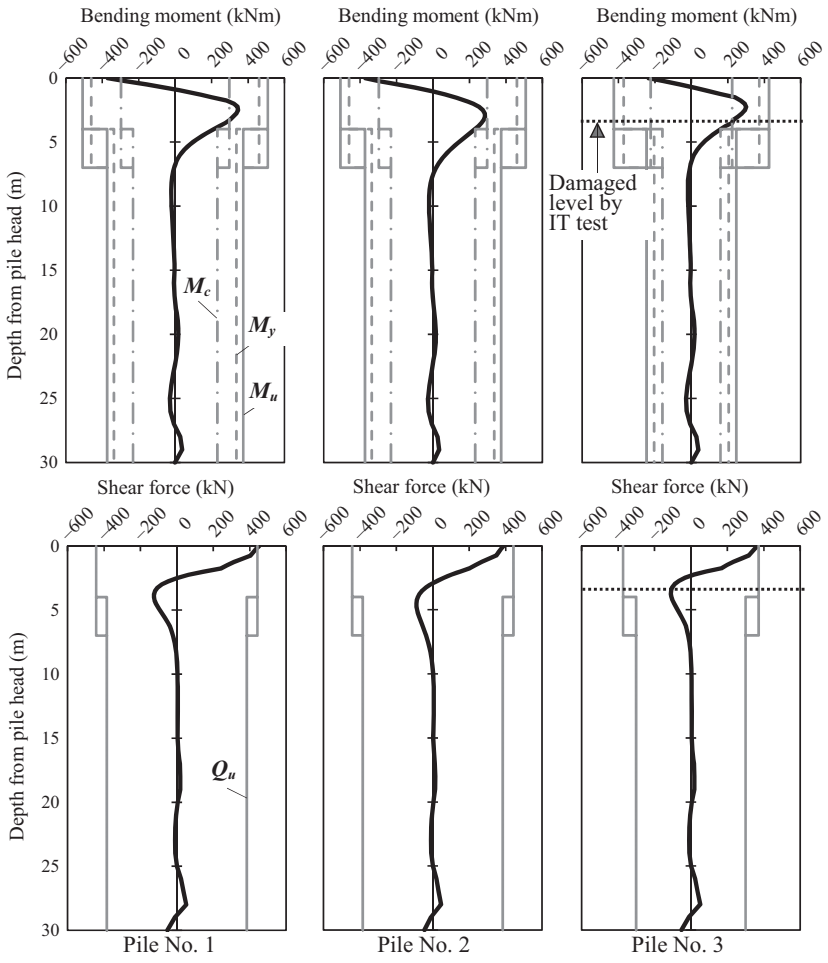

Figure 12. Bending moment and shear force distribution along pile in Case 1-1

Case 1-2B, where the pile group effect of Pile No. 2 is neglected, and in Case 1-2C, where excessive axial force is loaded solely on Pile No. 2, Pile No. 2 reaches bending capacity and Pile No. 6 reaches shear capacity. These results provide a fairly good representation of the damage observed in the pile foundations.

However, in Case 1-2A, where the pile group effect on Pile No. 2 is considered, Pile No.6 reaches shear failure, while the bending moment in Pile No. 2 does not reach yield level.

4.3 Results of West-to-East loading in Case 2 and East-to-West loading in Case 3

In Case 2, the loading from west to the east is simulated to represent the failure of Pile No. 1 and No. 2 due to the loss of bearing capacity against lateral load. The analysis considered that Pile No.6 could sustain lateral load even after Case 1 loading because the loading direction and depth of failure are different from Piles No. 1 and 2. Figure 14 shows the distribution of the bending moment and shear force in Piles

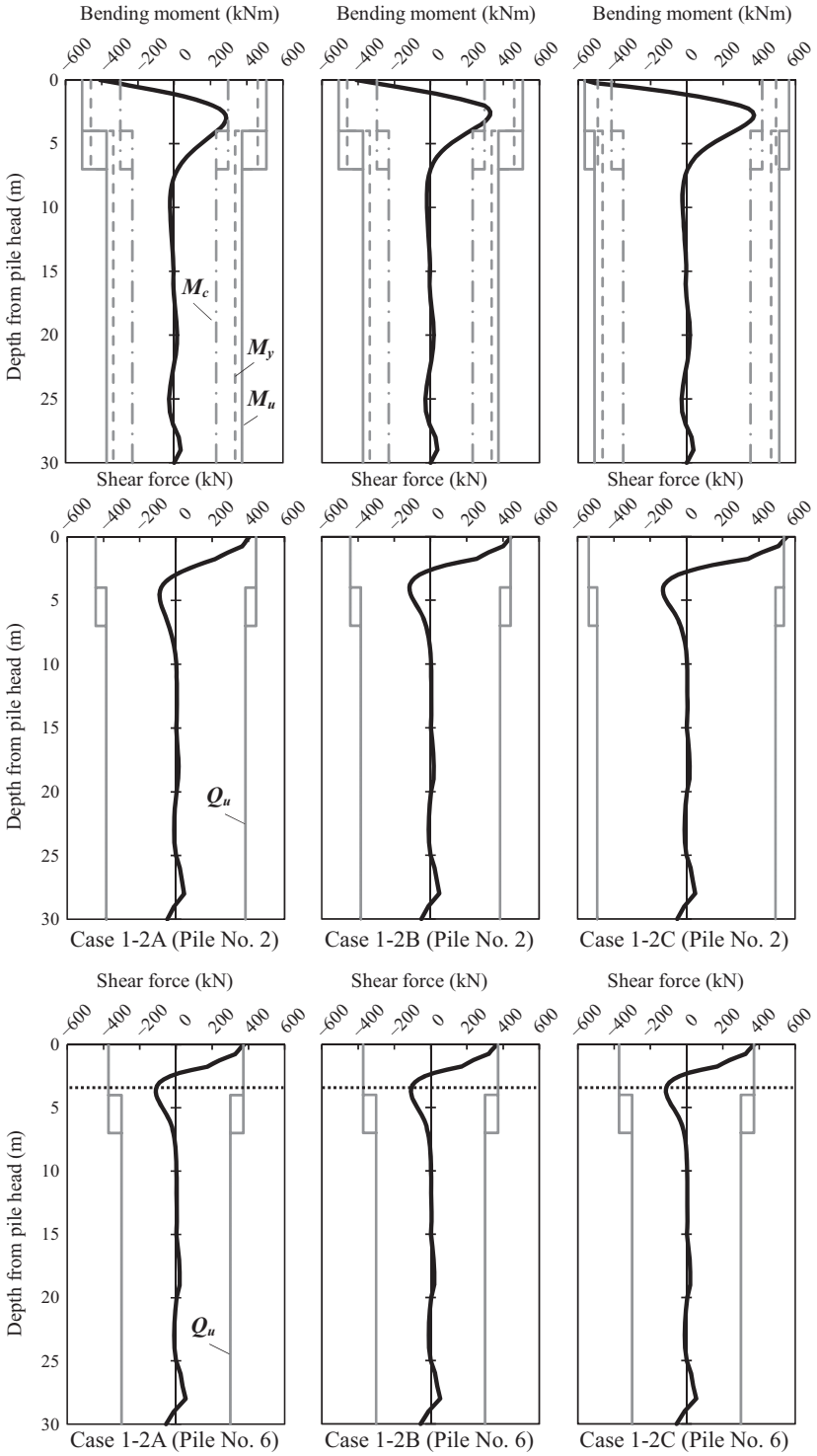

Figure 13. Bending moment and shear force of piles in Case 1-2

No. 5 to 8 at $C_B = 0.28$ and 0.34 in Case 2. At $C_B = 0.28$, the pile heads of Piles No. 6 and 8 reach shear capacity, and the middle parts of all the piles reach the yield moment. Thereafter, at $C_B = 0.34$, all the piles reach shear capacity at the pile heads and bending capacity at the middle parts. It is also possible that Piles No. 3 to 5 underwent tension failure at $C_B = 0.22$ since the axial forces obtained from the simulation model exceeded the tensile capacity of the piles after Piles No. 1 and No. 2 are considered as not supporting the vertical load.

Damage predicted from the simulation after $C_B = 0.28$ appears to be more severe than the observed damage. Based on the actual damage to the building's exterior walls, the upper limit of the input motion in the east-west direction corresponded to $C_B = 0.28$. However, the analyzed depth of cracking along the piles does not match the results of the ITs. This

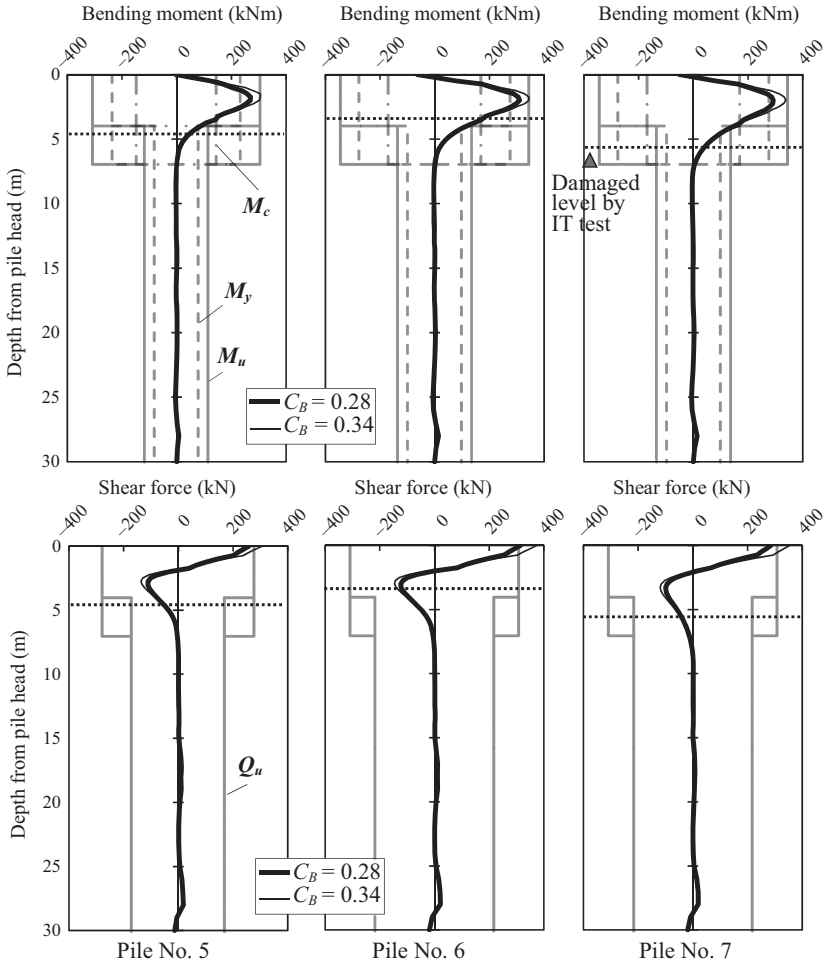

Figure 14. Bending moment and shear force of piles in Case 2

Table 4. Ratio of shared lateral load on each pile (unit: %)

Case	C_B	No. 1	No. 2	No. 3	No. 4	No. 5	No. 6	No. 7	No. 8
1-1	0.36	15.2	13.1	12.5	12.5	11.9	12.4	11.2	11.2
1-2A	0.39	-	15.6	14.7	14.7	14.1	14.5	13.2	13.2
1-2B	0.39	-	17.2	14.4	14.4	13.9	14.2	12.9	12.9
1-2C	0.39	-	20.4	13.9	13.9	13.3	13.7	12.4	12.4
2	0.34	-	-	14.3	15.2	15.8	18.7	17.3	18.7
3	0.34	13.5	12.8	12.4	10.8	13.1	13.1	13.1	11.4

Filled squares mean that they are the piles in the back considering the pile group effect.

outcome indicates a need for a closer examination of the nonlinear soil springs near the pile head area and more detailed interpretation of the IT results.

In Case 3, where load is applied in the east-to-west direction and the building is tilted, the piles do not reach failure even at $C_B = 0.34$ because the piles in baseline 1 are relatively strengthened by the increased axial loads. This result indicates that tilting and settlement of the building could have occurred after the complete failure of the piles in baseline 1.

Table 4 summarizes the percentage of lateral load shared by various piles in each of the simulated cases. The results indicate that the leading (front) piles and the piles that support higher axial load tend to share a higher percentage of the lateral load.

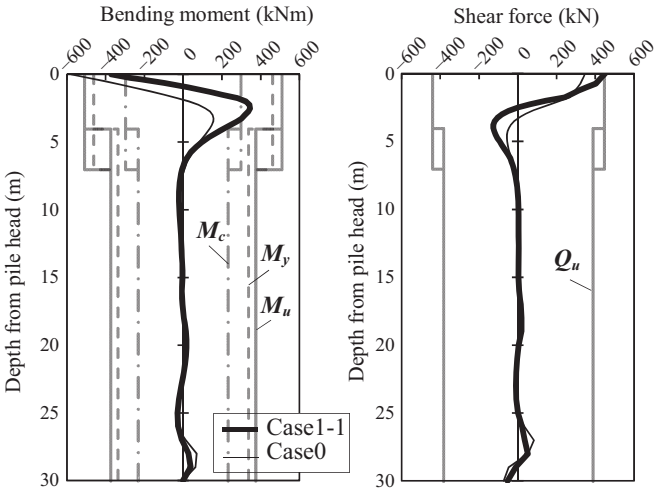

Figure 15. Comparison between Case 1-1 and Case 0 (Pile No. 1)

Based on the previously described analytical results, the analytical procedure that considered 2 phases of the damage process provides a fairly good explanation of the actual damage at the pile heads of Piles No. 1, 2, and 6, and at the middle parts of Piles No. 3 to 8. The analyses confirm that a suitable modeling of axial forces and soil springs is of primary

importance in evaluating the failure process of piles since the bending moment and shear force generated in piles during earthquakes heavily depend on those characteristics.

In this study, the axial force is treated as a constant maximum value. In reality, the axial force and the horizontal load should be represented as mutually interrelated. However, the approach used here is considered useful for design practice because an established approach for the quantitative evaluation of pile foundation performance is unavailable. In addition, a simulation that accounts for successive interrelation between horizontal and vertical loads is too complicated for practical purposes.

4.4 Influence of modeling

Figure 15 compares the results of Case 0 at $C_B = 0.36$ with Case 1-1, in which Pile No. 1 reaches shear capacity. Based on the pile elasticity model used in Case 0, the obtained bending moment exceeds ultimate the bending capacity, while the shear force remains within the shear capacity. Although simple to implement, elastic models may appear to provide a higher safety margin for design while not being representative of the actual damage observed. In consideration of the intense level of earthquake shaking, such simple methods are not considered applicable for design.

5. Conclusions

(1) The authors conducted seismic analyses to simulate the distinctive damage process of pile foundations where the characteristics of pile damage were observed to vary depending on pile position even in the same building and the same building frame, during the 2011 off the Pacific coast of Tohoku earthquake. The analysis results provide a reasonable explanation of the observed damage. The analysis model considered for the foundation structure provides a reliable evaluation of nonlinear behavior of the pile-soil system. The pile group effect is also taken into account depending on the pile position in relation to the loading direction.

(2) The analysis method considered 2 phases of the damage process to provide an efficient trace of the observed damage to piles. In Phase 1, the axial loads in Piles No. 1 and 2 increased under north-to-south loading, and the shares of horizontal load also increased, resulting in compression or shear failure at the pile head.
In Phase 2, the remaining piles were subjected to pull-up forces under the sequence of the west-to-east loading, reduction in the rotational stiffness at the pile head, and damage to the middle part of the piles.

(3) There is high possibility that partial and consecutive damage occurs during severe earthquakes, particularly when building has an irregular shape and/or unequal load distribution. Design based on simplified method that assumes elastic behavior of piles, fixed conditions at the pile head, and constant soil springs, is completely inadequate in representing the pile damage mechanism. It is necessary to consider nonlinear load-deformation characteristics of piles, to construct an adequate model of the pile head connection with respect to axial load and to take into account the nonlinear behavior of soil springs including pile group effects for seismic design pile foundations, particularly while considering severe earthquake shaking. It should be noted that the influence of axial load is remarkable.

In the comparatively simple approach to design proposed here, axial load is treated as constant at a maximum value. In addition, the lateral and axial loads at the pile head are estimated based on a static elasticity analysis of the superstructure. To refine the proposed method, it is necessary to identify the influence of these analysis conditions through parametric studies.

Acknowledgments

This study was initiated based on the collaborative research known as "The promotional project for upgrading the building code of Japan" supported by the Ministry of Land, Infrastructure, Transport, and Tourism during 2012 to 2013 and research on the "Development of performance-based seismic design for government office buildings and evacuation facilities with post-earthquake functional use" in association with the Building Research Institute, Chiba University, Yamaguchi University, Shibaura Institute of Technology and Toda Corporation. The authors would like to thank everyone involved for their cooperation.

Disclosure

The authors have no conflict of interest to declare.

References

1 Kaneko O, et al. Situations and analysis of damage to pile foundations of buildings in the 2011 Great east Japan earthquake, The JGS Journal, vol.62, No.1, 16-19, 2012.1 (in Japanese).
2 Kaneko O, Nakai S. Evaluation of seismic performance of pile foundations damaged during the 2011 Great east Japan earthquake, J. Struct. Constr. Eng., AIJ, Vol.79 No.695, 83-91, 2014.11 (in Japanese).
3 Shirinashihama S, et al. A repair and seismic retrofit case of an apartment building with damaged pile foundations during the great east Japan earthquake, Concrete Journal 53(3), 283-288, 2015 (in Japanese).
4 Imazu M, Fukutake K. Dynamic shear modulus and damping of gravel materials, Proc. of the 21st Japan national conference on soil mechanics and foundation engineering, 509-512, 1986 (in Japanese).
5 Dynamic analyses and seismic design, Vol.2 Procedure of dynamic analyses, edited by JSCE, Gihodo-shuppan, 281-282, 1989 (in Japanese).
6 Mase T, Nakai S. Examination of soil spring setting method of single pile, J. Struct. Constr. Eng., AIJ, No.680, 1527-1535, 2012.10 (in Japanese).
7 Nakai S, Kishida H. Non-linearity of relationship between subgrade reaction and displacement, The JGS Journal, vol.25, No.8, 21-28, 1977.8 (in Japanese).
8 Tabei T. The actual state of geotechnical parameters estimated from N-value and a future trend, Papers for panel discussion on foundation structure in annual meeting AIJ, 44, 2013.8 (in Japanese).
9 Recommendations for design of building foundations, AIJ, 280-284, 2001.10 (in Japanese).
10 Design manual for foundation structure with precast concrete pile, edition for buildings, Concrete Pile Installation Technology Association, 55-60, 2009.5 (in Japanese).
11 Kaneko O, et al. The flexural strength and deformation characteristics of precast concrete piles for estimation of seismic performance against severe earthquakes, J. Technol. Des., AIJ, Vol. 21, No.47, 95-98, 2015.2 (in Japanese).
12 Kaneko O, et al. A study on damage and its factor of pile foundations during the 2011 off the Pacific coast of Tohoku earthquake, Part 3 Experiment of lateral bearing capacity and deformability of pile foundations, Summaries of technical papers of annual meeting AIJ, B-1, 699-700, 2014.9 (in Japanese).
13 Specifications for highway bridges part4 substructures, Japan Road Association, 425, 2012.3 (in Japanese).
14 Kishida S, et al. The calculation method for the ultimate shear strength of large diameter PHC piles, J. Struct. Constr. Eng., AIJ, No.532, 103-110, 2000.6 (in Japanese).
15 Recommendations for design of building foundations, AIJ, 276-277, 2001.10 (in Japanese).

How to cite this article: Kaneko O, Kawamata S, Nakai S, Sekiguchi T, Mukai T. Analytical study of the main causes of damage to pile foundations during the 2011 off the Pacific coast of Tohoku earthquake. *Jpn Archit Rev.* 2018;1:235–244. https://doi.org/10.1002/2475-8876.12033